nature physics

SUPPLEMENTARY INFORMATION

DOI: 10.1038/NPHYS2731

Harnessing nuclear spin polarization fluctuations in a semiconductor nanowire

P. Peddibhotla[1], F. Xue[1], H. I. T. Hauge[2], S. Assali[2], E. P. A. M. Bakkers[2,3], M. Poggio[1]

[1]*Department of Physics, University of Basel, 4056 Basel, Switzerland*

[2]*Department of Applied Physics, Eindhoven University of Technology, 5600 MB Eindhoven, The Netherlands*

[3]*Kavli Institute of Nanoscience, Delft University of Technology, 2600 GA Delft, The Netherlands*

(Dated: July 14, 2013)

DOI: 10.1038/NPHYS2731

NOISE FLUCTUATIONS IN NANOSCALE NUCLEAR SPIN ENSEMBLES

Let us consider a small ensemble of noninteracting nuclear spins which are stochastically polarized. The nuclear spins of this ensemble are randomly oriented and the nuclear polarization varies in time. The Hamiltonian of the ensemble in an external magnetic field $\mathbf{B}_0$ along $\hat{e}_z$ can be written as,

$$\mathcal{H} = -\hat{\mathbf{M}} \cdot \mathbf{B}_0 = -\hat{M}_z B_0 = -\gamma B_0 \sum_j \hat{I}_{j,z}, \tag{1}$$

where $\hat{M}_z$ is the operator for the z-component of magnetization, γ is the gyromagnetic ratio, $\hat{I}_{j,z}$ is the operator for the z-component of spin for the jth nucleus, and the sum is over all the nuclei in the ensemble. For nuclei in experimentally applicable magnetic fields and temperatures, the difference between their energy levels is much less than the thermal energy, i.e. $\hbar\gamma B_0 \ll k_B T$. In this limit, a spin ensemble of N nuclei may be described by a density matrix $\hat{\rho} = \frac{\hat{1}}{(2I+1)^N}$. As a result, the root-mean-square (rms) value of the statistical magnetization is,

$$\sigma_{M_z} = \sqrt{\langle \hat{M}_z^2 \rangle - \langle \hat{M}_z \rangle^2} \tag{2}$$

$$= \sqrt{N \frac{I(I+1)}{3}} \hbar\gamma. \tag{3}$$

The operator $\hat{M}_z$ may be considered on a similar footing to the random, classical magnetization and replaced by a scalar M_z. In the large N limit, the probability density of $M_z = m$ is given by a Gaussian function [1],

$$f_{M_z}(m) = \frac{1}{\sqrt{2\pi}\sigma_{M_z}} e^{-\frac{m^2}{2\sigma_{M_z}^2}}. \tag{4}$$

DETECTION VOLUME AND NUMBER OF SPINS

Magneto-static model

We determine $\mathbf{B}_0(\vec{r})$ using a method employed in other recent MRFM experiments [2, 3]. First, we measure B_0 at several different positions above the Dy tip. The maximum value of f_{RF} for which a ^{1}H signal is obtained corresponds to the frequency where the resonant slice barely intersects hydrocarbon surface layer closest to the Dy tip. At this frequency $f_{\mathrm{RF,max}}$, $B_0(\vec{r}_0) = \frac{2\pi}{\gamma} f_{\mathrm{RF,max}}$ where $\vec{r}_0$ is the position of the hydrocarbon layer closest to the Dy tip. Several such measurements of B_0 at different $\vec{r}_0$ are then used to calibrate a three-dimensional magneto-static model of the Dy tip, as shown in Fig. S1. We measure the geometry of the Dy tip from SEM images, like the one shown in Fig. S3, and approximate it as a truncated cone of the appropriate dimensions. We then fine tune the volume magnetization in order to produce a field profile $\mathbf{B}_{\mathrm{tip}}(\vec{r})$ which agrees with the measured values of $B_0(\vec{r}_0) = |\mathbf{B}_{\mathrm{ext}} + \mathbf{B}_{\mathrm{tip}}(\vec{r}_0)|$ for our known applied field $\mathbf{B}_{\mathrm{ext}}$. At the operating field $B_{\mathrm{ext}} = 6$ T, we find a magnetization of 1.2×10^6 A/m, which is far below the maximum theoretical value of 2.4×10^6 A/m, but close to what was measured by Mamin et al. in similar Dy tips [4]. Our approximate model then gives us the ability to calculate both $B_0(\vec{r})$ and $\frac{\partial B_0}{\partial x}(\vec{r})$ at any position $\vec{r}$.

Lower limit on number of spins

A lower bound on the number of nuclear spins N_{lower} contributing to a MRFM signal can be set for small detection volumes. When the magnetic field gradient $\partial B_0/\partial x$ varies slowly over the detection volume, it can be treated as a constant for the nuclear spins contained therein. The measured force variance is then given by,

$$\sigma_S^2 = N \frac{I(I+1)}{3} (\hbar\gamma)^2 \left(\partial B_0/\partial x\right)^2, \tag{5}$$

where N is the number spins. Although the detection volumes in our experiments are small, this treatment represents an idealized picture, i.e. there is always some spatial variation of $\partial B_0/\partial x$ over the detection volume. Therefore, using our magneto-static model for $\mathbf{B}_0(\vec{r})$, we find the maximum value of $G_{\mathrm{max}} = |\partial B_0/\partial x|$ at the position of the sample. We then solve for the number of spins required in a gradient G_{max} to produce the measured force variance

DOI: 10.1038/NPHYS2731

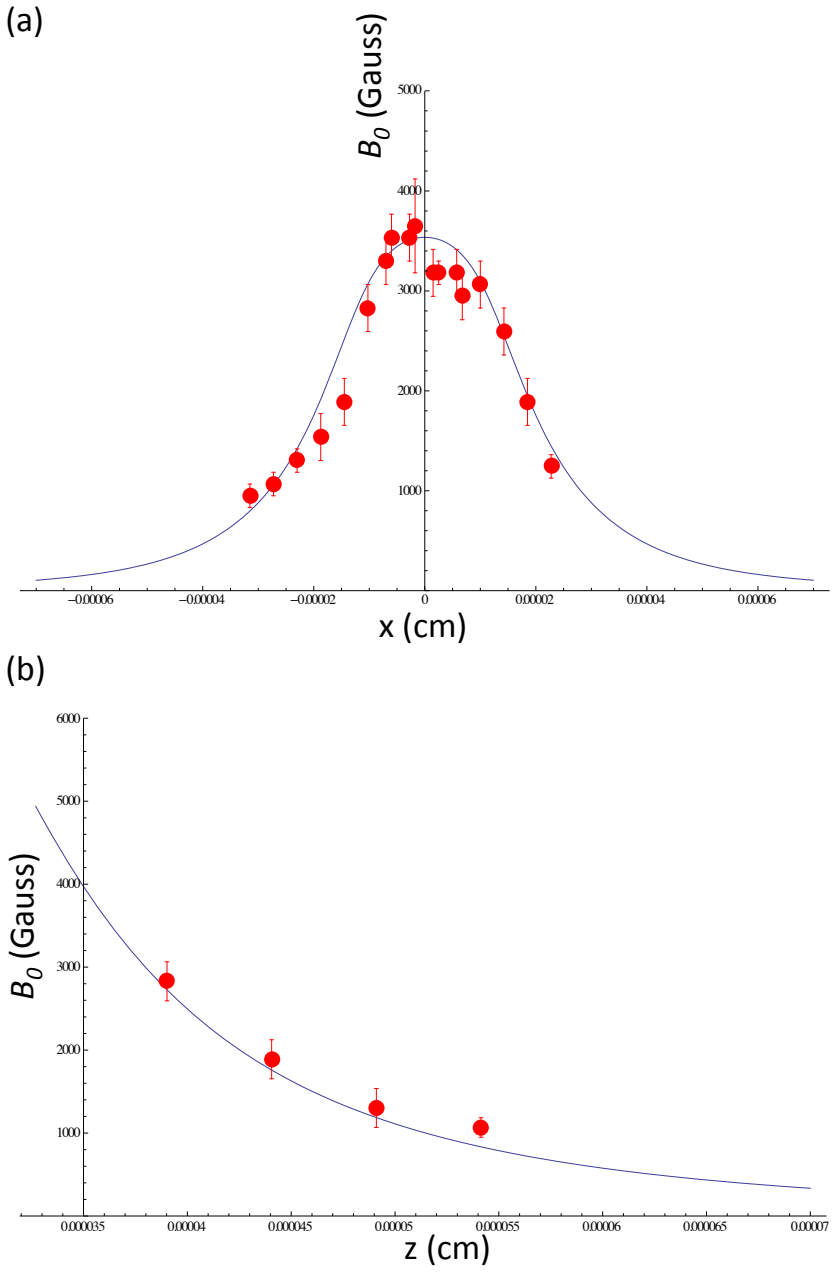

FIG. 1: **Measurements of B_0 as a function of position.** (a) The filled circles show B_0 measured by MRFM of the hydrocarbon layer on the surface of the GaP NW. The measured field is shown as a function of lateral position x of the closest hydrogen surface layer with respect to the center of the Dy nanomagnet. The end of the sample is held at a fixed height $z = 365$ nm above the microwire surface, or 85 nm above the top of the Dy tip. The solid line represents the output of our model for $\mathbf{B}_0(\vec{r})$. (b) Here we show B_0 measured by MRFM and calculated from our model as a function of the vertical position z at a fixed $x = 50$ nm from the center of the Dy tip.

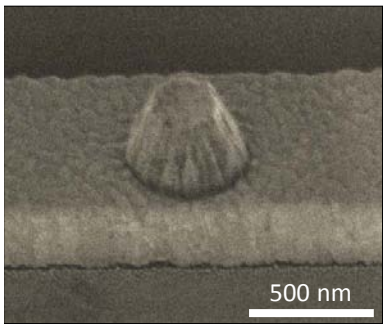

FIG. 2: **Dy nanomagnetic tip on Au microwire RF source.** This SEM depicts the lithographically produced Dy tip used to produce large spatial magnetic field gradients. This tip was used in the GaP NW experiment and measures 280 nm in height, 250 nm in upper diameter, and 500 nm in lower diameter. Beneath the tip is the 200-nm-thick and 1-μm-wide Au microwire for producing the transverse RF $\mathbf{B}_1(t)$ field.

σ_S^2:

$$N_{\text{lower}} = \frac{3}{I(I+1)} \left(\frac{\sigma_S^2}{(\hbar\gamma)^2 G_{\text{max}}^2} \right). \tag{6}$$

N_{lower} represents a lower bound since parts of the spin ensemble are exposed to gradients smaller than the local maximum and therefore contribute reduced force variances. Furthermore, (6) assumes that all the force variance produced by flipping spins is successfully measured by our apparatus; in reality, depending on the correlation time of the statistical spin polarization, some fraction of the signal can fall outside the bandwidth of the measurement.

Upper limit on number of spins

In order to set an upper bound on the number of nuclear spins in our detection volume, N_{upper}, we require knowledge both of the spatial dependence of $B_0(\vec{r})$ and of the shape and position of the sample. Since $B_0(\vec{r})$ is strongly inhomogeneous, there is a specific region in space at which the magnetic resonance condition is met for each center frequency $f_{\text{RF},0}$ of the transverse magnetic field $B_1(t)$. Only spins near these positions are adiabatically inverted and therefore included in the MRFM detection volume. This so-called "resonant slice" is a shell-like region in space above the magnetic tip whose thickness is determined by the magnetic field gradient and the modulation amplitude $\Omega_{\text{RF}}/(2\pi)$ of the frequency sweeps.

DOI: 10.1038/NPHYS2731

We can specify this region using an effective field model for adiabatic rapid passage in the manner of Section 4 of the supporting information in Degen et al [2]. This treatment shows that the spatial extent of the resonant slice can be described using the function:

$$\begin{aligned} \eta(\vec{r}) &= \left(1 - \tfrac{\gamma B_0(\vec{r}) - 2\pi f_{\mathrm{RF}}}{\Omega_{\mathrm{RF},0}}\right) \quad \text{for } (\gamma B_0(\vec{r}) - 2\pi f_{\mathrm{RF},0}) < \Omega_{\mathrm{RF}} \\ \eta(\vec{r}) &= 0 \qquad\qquad\qquad\quad \text{for } (\gamma B_0(\vec{r}) - 2\pi f_{\mathrm{RF},0}) \geq \Omega_{\mathrm{RF}}. \end{aligned} \tag{7}$$

$\eta(\vec{r})$ is normalized to 1 for a nuclear spin positioned exactly in the middle of the resonant slice ($\gamma B_0(\vec{r}) = 2\pi f_{\mathrm{RF},0}$), signifying that this spin is fully flipped by the adiabatic passage waveform and contributes its full force to the MRFM signal. A slightly off-resonant spin with $1 > \eta(\vec{r}) > 0$ is partially flipped and contributes a fraction of its full force to the MRFM signal. Spins outside the resonant slice with $\eta(\vec{r}) = 0$ contribute no signal.

In order to determine the number of spins within the detection volume V_{det}, we must determine the intersection of the resonant slice with the sample. By integrating the function $\eta(\vec{r})$ over the sample volume V_{S}, we can calculate V_{det} and the number of spins contained therein,

$$N_{\mathrm{upper}} = nV_{\mathrm{det}} = n\int_{V_{\mathrm{S}}} \eta(\vec{r})dV, \tag{8}$$

where n is the number density of the relevant nuclear spin. N_{upper} represents an upper limit because real-world ARP pulses are not ideal, meaning that not all the spins within V_{det} are likely to be periodically inverted. Furthermore, real-world sample geometries contain vacancies, defects, and roughness which cannot be accurately described by the idealized volume V_{S}.

We can confirm that this model corresponds to the measurement, by calculating the upper limit of the force variance on the cantilever $\sigma^2_{S,\mathrm{upper}}$ produced by this volume of nuclear spins. Since the magnetic field gradient varies throughout the resonant slice, equal numbers of nuclei at different positions in the slice contribute different forces to the final signal. Using (3) and (7), we find the total MRFM force variance:

$$\sigma^2_{S,\mathrm{upper}} = \int_{V_{\mathrm{S}}} \eta(\vec{r}) \left(\frac{\partial B_0(\vec{r})}{\partial x}\right)^2 n\frac{I(I+1)}{3}(\hbar\gamma)^2 dV. \tag{9}$$

This calculation sets an upper bound on the measured force variance for two principal reasons: first, it assumes that idealized (the maximum) number of nuclear spins contribute

to the force variance; second, as in the previous section, we assume that all the force variance produced by flipping spins is successfully measured, i.e. none of the signal falls outside of the measurement bandwidth.

In order to calculate N_{upper} and $\sigma^2_{S,\mathrm{upper}}$ for each experiment, we set f_{RF} and Ω_{RF} according to the parameters of the ARP pulses. Furthermore, we model both the shape and position of the NW sample and the profile of the static magnetic field $B_0(\vec{r})$. Given our knowledge of the shape of the NW sample from SEM images such as Fig. S5, we make an idealized approximation of the sample volume V_{S}. The NWs are modeled as cylindrical solids with the diameters matching the diameters seen in the SEMs. The hydrocarbon layer is modeled as a thin film on the surface of this solid. All dimensions are meant to match the cross-sectional size of the NW as it is closest to the Dy tip, since this part of the sample contributes all of the observed σ^2_S. The back part of the sample, with larger cross-sectional area, contributes no signal since it lies mostly outside of the tiny resonant slice. Even if this distant part of the sample were in the slice, it would contribute a vanishingly small σ^2_S due to the rapid decrease in $\left|\frac{\partial B_0}{\partial x}\right|$ as a function of distance from the Dy tip.

Calculations

For experiments on ^{31}P in the InP NW, we measure $\sigma^2_S = 50$ aN^2. Given that $G_{\mathrm{max}} = 1.5\times 10^6$ T/m, $N_{\mathrm{lower}} = 6\times 10^5$. Numerical integration of (8) and (9) results in $N_{\mathrm{upper}} = 1\times 10^7$ and $\sigma^2_{S,\mathrm{upper}} = 190$ aN^2.

For experiments on ^{31}P in the GaP NW, we measure $\sigma^2_S = 43$ aN^2. Given that $G_{\mathrm{max}} = 1.5\times 10^6$ T/m in this experiment as well, $N_{\mathrm{lower}} = 7\times 10^5$. Numerical integration of (8) and (9) results in $N_{\mathrm{upper}} = 3\times 10^7$ and $\sigma^2_{S,\mathrm{upper}} = 380$ aN^2.

For experiments on ^{1}H on the same GaP NW, we measure $\sigma^2_S = 72$ aN^2. Given that $G_{\mathrm{max}} = 1.5\times 10^6$ T/m, $N_{\mathrm{lower}} = 2\times 10^5$. For the numerical integration of (8) and (9) we model the hydrocarbon layer as a 2-nm-thick shell around an idealized cylindrical NW. This thickness is consistent with the thickest estimate used in previous calculations of such layers, which estimated thicknesses between 1 and 2 nm [2, 3, 5]. Our calculation results in $N_{\mathrm{upper}} = 7\times 10^5$ and $\sigma^2_{S,\mathrm{upper}} = 220$ aN^2.

The discrepancy between $\sigma^2_{S,\mathrm{upper}}$ and the measured force variance is likely the result of our approximate knowledge of the sample's nanometer-scale morphology. Our highly

DOI: 10.1038/NPHYS2731

idealized model geometry is surely a poor approximation of the true experimental volume, in particular for the case of a hydrocarbon adsorption layer which is certainly not uniform. For this reason, we choose to specify N_{lower} and N_{upper} by two different methods, rather than providing a single estimate for the number of spins.

CANTILEVER INDUCED NUCLEAR SPIN RELAXATION

The high sensitivity of the MRFM technique used in our experiments implies a strong coupling between the nuclear magnetic moments in the detection volume and the motion of the cantilever sensor. In fact, the spin correlation time in the experiment, τ_m, is limited by the magneto-mechanical noise originating from the thermal motion of the cantilever [6–10].

In a strong static field $\mathbf{B}_0$, nuclear spin and mechanical spin degrees of freedom are well decoupled since the spin precession frequency is orders of magnitude larger than typical cantilever frequencies. In this situation, at the cryogenic temperatures of our experiment, the nuclear spin relaxation time T_1 can be as long as several hours. In the presence of a near resonant transverse magnetic field $\mathbf{B}_1(t)$ at a frequency f_{RF}, however, kHz-frequency noise that overlaps with the Rabi frequency of the spin will induce spin relaxation. The spins in the sample attached to the cantilever experience a magnetic field noise $\mathbf{B}_n(t) = \frac{\partial \mathbf{B}_{\mathrm{tip}}}{\partial x} x(t)$ around these frequencies due to the random thermal motion $x(t)$ of the cantilever. The total magnetic field at the position of the spin is $\mathbf{B}_0^{'}(t) = \mathbf{B}_0 + \mathbf{B}_n(t)$. Then, in the reference frame that rotates with angular frequency $\omega = 2\pi f_{\mathrm{RF}}$ near resonance, the spin experiences an effective magnetic field,

$$\mathbf{B}_{\mathrm{eff}}^{'}(t) = \left(B_0 - \frac{2\pi f_{\mathrm{RF}}}{\gamma} + B_{n,z}(t) \right) \mathbf{e}_z + \frac{1}{2} B_1 \mathbf{e}_x, \tag{10}$$

where γ is the gyromagnetic ratio. We have neglected both the counter-rotating component of the transverse field and the transverse components of the magnetic field noise. In both cases we can invoke the rotating wave approximation since these fields oscillate so quickly that their effect is negligible. Built into this approximation is the assumption that, as in most experimental situations, the magnetic field noise falls off strongly as a function of frequency. When we consider a transverse field $\mathbf{B}_1(t)$ of fixed amplitude and frequency, we can write the Hamiltonian of a spin in the rotating frame as

$$\mathcal{H}(t) = -\hat{\mu}.\mathbf{B}_{\mathrm{eff}}^{'}(t) = \mathcal{H}_0 + \mathcal{H}_1(t), \tag{11}$$

where

$$\begin{aligned} \mathcal{H}_0 &= -\gamma\hbar \left[\left(B_0 - \frac{2\pi f_{\mathrm{RF}}}{\gamma} \right) \hat{I}_z + \frac{1}{2} B_1 \hat{I}_x \right] \\ \mathcal{H}_1(t) &= -\gamma\hbar B_{n,z}(t) \hat{I}_z, \end{aligned} \tag{12}$$

DOI: 10.1038/NPHYS2731

where $\hat{I}_z$ is the nuclear spin operator along $\hat{z}$. In the simplest case of a spin-1/2 system, the eigenstates of operator $\hat{I}_z$ may be denoted by $|\uparrow_z\rangle$ and $|\downarrow_z\rangle$ with eigenvalues $\pm 1/2$. Without any time-dependent perturbation, the spins are quantized along the effective field with an energy spacing,

$$\hbar\omega_{\rm eff} = \gamma\hbar B_{\rm eff} = \gamma\hbar\left[\left(B_0 - \frac{2\pi f_{\rm RF}}{\gamma}\right)^2 + \frac{1}{4}B_1^2\right]^{\frac{1}{2}}. \tag{13}$$

$|\uparrow_n\rangle$ and $|\downarrow_n\rangle$ are the eigenstates of $\hat{\mathbf{I}}\cdot\mathbf{e}_n$, where $\mathbf{e}_n$ is a unit vector that makes a polar angle θ with $\mathbf{e}_z$ and an azimuthal angle ϕ with $\mathbf{e}_x$. at $t = 0$, let the energy eigenstate be $|\uparrow_n\rangle$ where $\sin\theta = \frac{B_1}{2B_{\rm eff}}$. We wish to find $C_{\uparrow_n}(t)$ and $C_{\downarrow_n}(t)$ such that

$$|\Psi(t)\rangle = C_{\uparrow_n}(t)e^{i\frac{\omega_{\rm eff}}{2}t}|\uparrow_n\rangle + C_{\downarrow_n}(t)e^{-i\frac{\omega_{\rm eff}}{2}t}|\downarrow_n\rangle, \tag{14}$$

where $|\Psi(t)\rangle$ stands for the state of the system at time t. The transition probability for $|\uparrow_n\rangle \rightarrow |\downarrow_n\rangle$ is obtained from first-order time-dependent perturbation theory by $P_{\uparrow_n\downarrow_n}(t) = |C_{\downarrow_n}(t)|^2$ [11], where

$$\begin{aligned} C_{\downarrow_n}(t) &= -\frac{i}{\hbar}\int_0^t e^{i\omega_{\rm eff}t'}\langle\downarrow_n|\mathcal{H}_1(t')|\uparrow_n\rangle dt' \\ &= i\gamma\int_0^t e^{i\omega_{\rm eff}t'}B_{n,z}(t')\langle\downarrow_n|\hat{I}_z|\uparrow_n\rangle dt' \\ &= \frac{i\gamma\sin\theta}{2}\int_0^t e^{i\omega_{\rm eff}t'}B_{n,z}(t')dt' \qquad . \end{aligned} \tag{15}$$

The transition probability per unit time, i.e. the spin relaxation rate in the rotating frame is therefore:

$$\begin{aligned} T^{-1} &= \frac{d}{dt}\left(C_{\downarrow_n}(t)C^*_{\downarrow_n}(t)\right) \\ &= \left(\frac{d}{dt}C_{\downarrow_n}(t)\right)C^*_{\downarrow_n}(t) + C_{\downarrow_n}(t)\left(\frac{d}{dt}C^*_{\downarrow_n}(t)\right) \\ &= \left(\frac{\gamma\sin\theta}{2}\right)^2\left(e^{i\omega_{\rm eff}t}B_{n,z}(t)\int_0^t e^{-i\omega_{\rm eff}t'}B_{n,z}(t')dt' + e^{-i\omega_{\rm eff}t}B_{n,z}(t)\int_0^t e^{i\omega_{\rm eff}t'}B_{n,z}(t')dt'\right) \\ &= \left(\frac{\gamma\sin\theta}{2}\right)^2\left(\int_0^t e^{i\omega_{\rm eff}(t-t')}B_{n,z}(t)B_{n,z}(t')dt' + \int_0^t e^{-i\omega_{\rm eff}(t-t')}B_{n,z}(t)B_{n,z}(t')dt'\right). \end{aligned} \tag{16}$$

Due to the random nature of $B_{n,z}(t)$, it is only possible to calculate stochastic expectation values $\langle B_{n,z}(t)B_{n,z}(t')\rangle$. If the stochastic process is assumed to be stationary and $\tau = t' - t$,

then,

$$
\begin{aligned}
T^{-1} &= \left(\frac{\gamma \sin\theta}{2}\right)^2 \left(\int_{-t}^{0} e^{-i\omega_{\text{eff}}\tau} \langle B_{n,z}(t) B_{n,z}(t+\tau)\rangle d\tau + \int_{-t}^{0} e^{i\omega_{\text{eff}}\tau} \langle B_{n,z}(t) B_{n,z}(t+\tau)\rangle d\tau\right) \\
&= \left(\frac{\gamma \sin\theta}{2}\right)^2 \left(\int_{-t}^{t} e^{-i\omega_{\text{eff}}\tau} \langle B_{n,z}(t) B_{n,z}(t+\tau)\rangle d\tau\right) \\
&\approx \left(\frac{\gamma \sin\theta}{2}\right)^2 \left(\int_{-\infty}^{\infty} e^{-i\omega_{\text{eff}}\tau} \langle B_{n,z}(t) B_{n,z}(t+\tau)\rangle d\tau\right) \\
&= \left(\frac{\gamma \sin\theta}{2}\right)^2 2\pi S_B(\omega_{\text{eff}}) \\
T^{-1} &= \frac{\pi\gamma^2}{2}\left(\frac{B_1}{2B_{\text{eff}}}\right)^2 S_B(\omega_{\text{eff}}),
\end{aligned}
\tag{17}
$$

where $S_B(\omega)$ is the spectral density of $B_{n,z}(t)$. The assumption of the approximate equality is justified because the relevant times t can be significantly longer than the correlation time of the thermal motion. The result shows that the spectral density of the magnetic field noise at ω_{eff} determines the rotating frame relaxation time T. For an exactly resonant transverse field, this relaxation rate is known as $T = T_{1\rho}$. Under these conditions, $\frac{B_1}{2B_{\text{eff}}} = 1$ and $\omega_{\text{eff}}/(2\pi) = \frac{\gamma}{4\pi}B_1$, which is typically in the kHz-range. Thus, $T_{1\rho}^{-1} = \frac{\pi\gamma^2}{2}S_B(\omega_{\text{eff}})$. The sensitivity of $T_{1\rho}$ to low frequency magnetic field noise, which is common in experimental situations, typically results in $T_{1\rho} \ll T_1$.

For our ARP pulses, the correlation time τ_m can be derived from a similar expression. In that case, we must take into account the time dependence of the amplitude and frequency of $B_1(t)$ during the ARP pulses; this dependence implies that both $B_{\text{eff}}(t)$ and $\omega_{\text{eff}}(t)$ will vary in time. We then assume that the relaxation rate can be described as the average rate over a frequency sweep,

$$
\tau_m^{-1} = \frac{\pi\gamma^2}{T_c}\int_0^{T_c/2}\left(\frac{B_1(t)}{2B_{\text{eff}}(t)}\right)^2 S_B\left(\omega_{\text{eff}}(t)\right) dt, \tag{18}
$$

where $T_c = 1/f_c$ is the oscillation period of the fundamental cantilever mode (in our protocol a single ARP sweep lasts for $T_c/2$). $f_{\text{RF}}(t)$ is swept from $\frac{1}{2\pi}(\gamma B_0 - \Omega_{\text{RF}})$ to $\frac{1}{2\pi}(\gamma B_0 + \Omega_{\text{RF}})$ during an ARP pulse. Since $\Omega_{\text{RF}} > \gamma B_1(t)$, the Rabi frequency $\omega_{\text{eff}}(t)/(2\pi)$ traverses a broad range of frequencies during the sweep. Therefore the critical difference between τ_m (the relaxation rate in the presence of ARP pulses) and $T_{1\rho}$ (the relaxation rate in the presence of a resonant transverse field) is that τ_m is sensitive to noise in a frequency band $\frac{\gamma}{4\pi}B_1 \leq \frac{\omega_{\text{eff}}}{2\pi} \lesssim \frac{\Omega_{\text{RF}}}{2\pi}$, while $T_{1\rho}$ is influenced by noise near $\frac{\gamma}{4\pi}B_1$ only. As a result, $\tau_m \leq T_{1\rho}$,

DOI: 10.1038/NPHYS2731

depending on the spectrum of the magnetic field noise in the experiment. In our experiments the main contribution to the magnetic field noise spectral density in the sensitive frequency band is produced by the thermal motion of the cantilever in the strong magnetic field gradient. In this case, $S_B(\omega) = \left(\frac{\partial B_{\mathrm{tip,z}}}{\partial x}\right)^2 S_x(\omega)$, where $S_x(\omega)$ is the spectral density of the cantilever thermal motion.

The nuclear spin relaxation rate during the ARP pulses, τ_m, sets the correlation time of the nuclear spin polarization fluctuations that we measure. The relaxation behind this process, as discussed above, is dominated by the random thermal motion of the cantilever. In particular, for the cantilever used in this experiment, thermal motion in mechanical modes beyond the fundamental mode is the most important. Since the amplitude of $B_1(t)$ is around 20 mT, relaxation will only be induced by mechanical modes (or other magnetic field noise) with frequencies greater than $\frac{\gamma}{4\pi}B_1 = 422$ kHz for ^{1}H and 172 kHz for ^{31}P. The resulting spin polarization fluctuations are assumed to be random. This assumption is supported by the fact that we measure a Gaussian distribution of spin polarizations, as shown in Fig. 2(b) (note that X is proportional to spin polarization). Likewise, Degen et al. [12], show that the autocorrelation function of spin fluctuations under this kind of relaxation is exponential. Both results are consistent with the production of statistically independent polarization ensembles during ARP pulses. We cannot rule out that the relaxation creates some order internal to the spin ensemble (i.e. dipolar order). Such order would not be reflected in our measurement of polarization and therefore would not affect the creation of statistically independent spin polarizations. Internal spin order should also be irrelevant to the potential use of our method in applications like the initialization of nanoscale samples for NMR or the hyperpolarization and narrowing of lattice spins nuclear spin distributions for solid state quantum dot experiments.

NARROWING OF NUCLEAR SPIN DISTRIBUTION

Let the spin fluctuation S and thermal fluctuation T be independent random variables that are normally distributed with mean zero and variance σ_S^2 and σ_T^2 respectively, i.e. the probability density of a spin fluctuation $S = s$ is given by $f_S(s) = N(0, \sigma_S^2)$ and the probability density of the thermal fluctuation $T = t$ is $f_T(t) = N(0, \sigma_T^2)$. Our measurement X contains both a spin fluctuation S and an additive and independent thermal noise fluctuation T. Since S and T are independent, the total fluctuation $X = S + T$ is also normally distributed, with the probability density of $X = x$ given by $f_X(x) = N(0, \sigma_S^2 + \sigma_T^2)$. The conditional probability density for the spin fluctuation $S = s$ given the occurrence of the total fluctuation $X = x$ is,

$$f_S(s|X=x) = \frac{f_T(x-s)f_S(s)}{f_X(x)} \tag{19}$$

$$f_S(s|X=x) = \frac{1}{\sqrt{2\pi}\frac{\sigma_S\sigma_T}{\sqrt{\sigma_S^2+\sigma_T^2}}} e^{-\frac{1}{2}\left(\frac{(x-s)^2}{\sigma_T^2}+\frac{s^2}{\sigma_S^2}-\frac{x^2}{\sigma_S^2+\sigma_T^2}\right)} \tag{20}$$

$$= \frac{1}{\sqrt{2\pi}\frac{\sigma_S\sigma_T}{\sqrt{\sigma_S^2+\sigma_T^2}}} e^{-\frac{1}{2}\left(\left(\frac{1}{\sigma_T^2}+\frac{1}{\sigma_S^2}\right)s^2-\frac{2sx}{\sigma_T^2}+\frac{x^2}{\sigma_T^2}-\frac{x^2}{\sigma_S^2+\sigma_T^2}\right)} \tag{21}$$

$$= \frac{1}{\sqrt{2\pi}\frac{\sigma_S\sigma_T}{\sqrt{\sigma_S^2+\sigma_T^2}}} e^{-\frac{1}{2}\left(\frac{1}{\sigma_T^2}+\frac{1}{\sigma_S^2}\right)\left(s^2-2s\frac{\sigma_S^2 x}{\sigma_T^2+\sigma_S^2}+\frac{\sigma_S^4 x^2}{\left(\sigma_S^2+\sigma_T^2\right)^2}\right)} \tag{22}$$

$$= \frac{1}{\sqrt{2\pi}\frac{\sigma_S\sigma_T}{\sqrt{\sigma_S^2+\sigma_T^2}}} e^{-\frac{\left(s-\frac{\sigma_S^2 x}{\sigma_T^2+\sigma_S^2}\right)^2}{2\frac{\sigma_S^2\sigma_T^2}{\sigma_S^2+\sigma_T^2}}}. \tag{23}$$

$$\tag{24}$$

Therefore, $f_S(s|X=x) = N(x\frac{\sigma_S^2}{\sigma_S^2+\sigma_T^2}, \frac{\sigma_S^2\sigma_T^2}{\sigma_S^2+\sigma_T^2})$. This result means that in our protocol for the capture and storage of spin fluctuations, given a total captured fluctuation X_c, we store a spin fluctuation with mean $\langle X_s \rangle = X_c\frac{\sigma_S^2}{\sigma_S^2+\sigma_T^2}$ and a variance $\sigma_{X_s}^2 = \frac{\sigma_S^2\sigma_T^2}{\sigma_S^2+\sigma_T^2}$.

When we retrieve this fluctuation by a second measurement of X, we once again measure both the spin signal and the thermal noise. The mean of this retrieval measurement is the same as the mean of the stored spin fluctuation, $\langle X_r \rangle = \langle X_s \rangle = X_c\frac{\sigma_S^2}{\sigma_S^2+\sigma_T^2}$, but the variance will include the additional thermal noise of the measurement: $\sigma_{X_r}^2 = \frac{\sigma_S^2\sigma_T^2}{\sigma_S^2+\sigma_T^2} + \sigma_T^2$.

DOI: 10.1038/NPHYS2731

WAIT TIME REQUIRED TO CAPTURE A FLUCTUATION

The fluctuation $X(t)$ is normally distributed and the probability density of $X = x$ is given by,

$$f_X(x) = \frac{1}{\sqrt{2\pi}\sigma_X} e^{-\frac{x^2}{2\sigma_X^2}}. \tag{25}$$

We are interested in finding the average time one has to wait before capturing a fluctuation X_c of $X(t)$. In order for such a fluctuation to be captured, $X(t)$ must cross X_c with positive (negative) slope for $X_c > 0$ ($X_c < 0$). As shown by Rice [13], the expected number of such passages per second is,

$$\frac{1}{2} n_0 e^{-\frac{X_c^2}{2\sigma_X^2}}, \tag{26}$$

where n_0 is the average number of zero-crossings per second. Therefore the average time to wait before capturing a fluctuation X_c is,

$$T_{\text{wait}} = \frac{2}{n_0} e^{\frac{X_c^2}{2\sigma_X^2}}. \tag{27}$$

In the limit of large SNR where σ_X is dominated by spin fluctuations, we can let $\sigma_X = \rho_S$ and solve for the achievable polarization:

$$\rho_c = \rho_S \sqrt{2 \ln\left(\frac{n_0}{2} T_{\text{wait}}\right)}. \tag{28}$$

In terms of N and I this equation reduces to,

$$\rho_c = \sqrt{\frac{1}{N} \frac{2(I+1)}{3I} \ln\left(\frac{n_0}{2} T_{\text{wait}}\right)}. \tag{29}$$

This result shows that the size of the captured polarization is independent of temperature and applied magnetic field and depends only on the number of spins in the ensemble N, the spin number I, n_0, which is closely related to the correlation time in the rotating frame, and T_{wait}. This statement is, in fact, only partially true. Two important limit exist in which this analysis fails. The first is for small applied magnetic field $B_0 \sim B_1$ or smaller, where the rotating wave approximation breaks down. B_1 must be large enough such that the ARP pulses are indeed adiabatic, e.g. in the experiments discussed here $B_1 > 5$ mT. The second limit is at high enough temperatures where T_1 in the lab frame is no longer long enough or no longer different enough from τ_m in the rotating frame for the capture protocol to work efficiently.

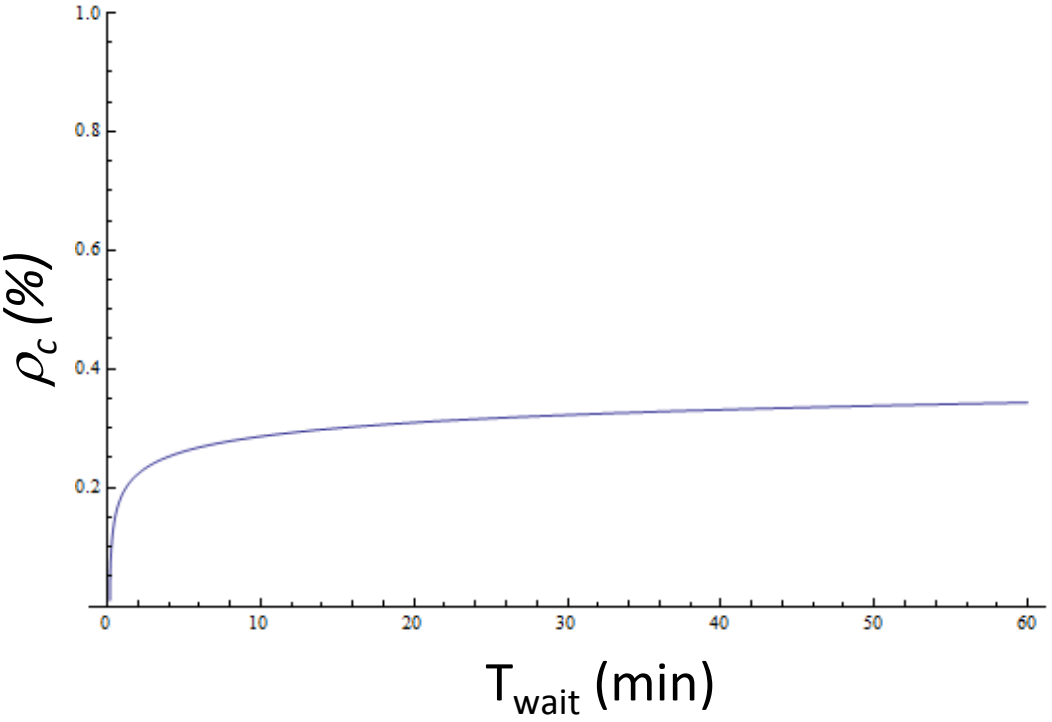

FIG. 3: **Potential captured polarization ρ_c as a function of wait time $T_{\mathbf{wait}}$.** This plot shows (29) for the parameters relevant to our experiment on a nanometer-scale ^{31}P ensemble in a nanowire as discussed in the manuscript: $N = 10^6$, $I = 1/2$, and $n_0 = 0.2$ Hz.

Nevertheless, it is instructive to write the polarization that can be captured shown in (29) in terms of the conventionally achievable thermal polarization ρ_B. As discussed previously, this expression is only valid for $B_0 \gg B_1$ and for T low enough that T_1 and τ_m meet the requirements of the capture protocol.

$$\rho_c/\rho_B = \frac{k_B T}{\hbar\gamma B_0}\sqrt{\frac{1}{N}\frac{6}{I(I+1)}\ln\left(\frac{n_0}{2}T_{\mathrm{wait}}\right)}. \tag{30}$$

From this relation, we see that the polarization of a nuclear spin ensemble by the capture of nuclear spin fluctuations can – in principle – be advantageous compared to using conventional thermal polarization for small samples (small N), for high temperature, and low magnetic field.

DOI: 10.1038/NPHYS2731

NANOWIRE GROWTH

InP nanowire growth

The InP NWs are grown with the vapor-liquid-solid (VLS) method in a low-pressure (50 mbar) Aixtron CCS-MOVPE reactor. The Au catalyst nanoparticles are dispersed using a 60-nm Au colloidal solution over the InP (111)B substrate. The InP NWs are grown at 420°C for 20 min using Tri-Methyl Indium (TMI) and Phosphine (PH_3) as precursor gases at molar fractions of 2.5×10^{-5} and 8.3×10^{-3}, respectively, with a total flow of 6.0 l/min using hydrogen as a carrier gas. The Arsine (AsH_3) gas (molar flow 3.3×10^{-4}) is introduced in the reactor chamber for 2 s in order to grow an InAsP quantum dot, followed by 20 min InP growth. The samples are then overgrown for 5 min at 500°C with a InP shell, using TMI and PH3 at molar fractions of 2.3×10^{-5} and 8.3×10^{-3}, respectively.

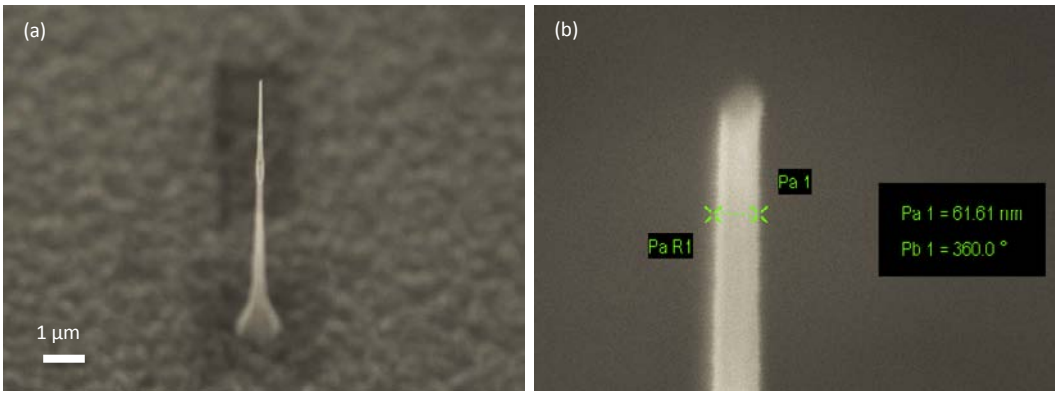

FIG. 4: **SEMs of a representative InP NW.** (a) This SEM depicts an as-grown InP NW before its attachment to the cantilever tip. (b) A second SEM shows a zoomed-in view of the narrow end of the NW, with the Au catalyst particle at the tip.

GaP nanowire growth

The GaP NWs are grown with the VLS method in a low-pressure (50 mbar) Aixtron CCS-MOVPE reactor, using Au nanocatalysts deposited in square arrays by e-beam lithography (25 nm - 100 nm diameter, 200 nm - 5 μm pitch) over a zinc blende GaP (111)B substrate [14]. The samples are annealed at 750°C for 8 min and then grown at 750°C for 13 min using Tri-Methyl Gallium (TMG) and Phosphine (PH_3) as precursor gases at molar fractions of

7.4×10^{-5} and 1.7×10^{-3}, respectively, with a total flow of 8.2 l/min using hydrogen as carrier gas. Hydrogen Chloride (HCl) gas (molar fraction 1.2×10^{-4}) is used to suppress the radial overgrowth in the NWs. In order to increase the NW diameter, the GaP shell growth is performed at 690°C for 22 min using TMG and PH_3 as precursor gases at molar fractions of 8.1×10^{-5} and 1.1×10^{-2}, respectively. Next, the $Al_{0.4}Ga_{0.6}P$ shell is grown for 5 min with TMG, TMAl and PH_3 as precursor gases at molar fractions of 2.7×10^{-5}, 1.5×10^{-5} and 1.1×10^{-2}, respectively. The tapered axial segment which can be seen at the top of the NWs is related to the parasitic decomposition of the precursors at the gold droplet during the shell growth.

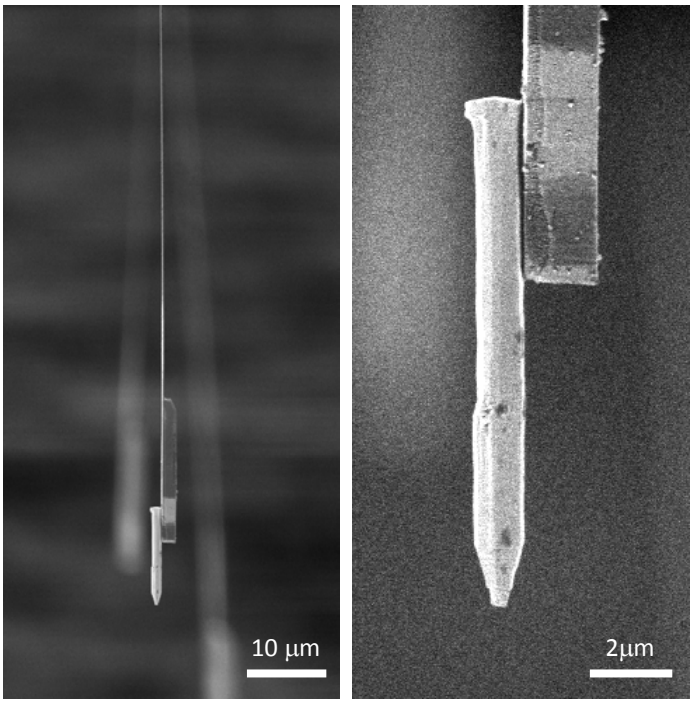

FIG. 5: **SEMs of the GaP NW on the cantilever tip.** (left) This SEM depicts the GaP NW affixed to the Si cantilever from the side. (right) A second SEM shows a zoomed-in view of the NW. The cantilever is 100-nm-thick with a 2-μm-thick and 17-μm-long mass at its end.

DOI: 10.1038/NPHYS2731

CONTROL AND CAPTURE PROTOCOL

The feedback used to rectify and narrow nuclear spin fluctuations in Fig. 3(a) is realized via a field-programmable gate array (FPGA) in conjunction with an arbitrary waveform generator (AWG). π-inversions are carried out by inserting an ARP pulse with a duration equivalent to a full cantilever cycle rather than the usual half-cycle. As a result, the spin ensemble's periodic inversion at the cantilever frequency undergoes a 180° phase shift. Since only fluctuations due to nuclear spins are affected by the π-inversions, the effectiveness of the protocol depends on the fraction of $X(t)$ arising from spin compared to thermal fluctuations, i.e. the larger the power signal-to-noise ratio (SNR) σ_S^2/σ_T^2 is, the more effective the control of $X(t)$ will be. The capture of large fluctuations, shown in Figs. 4 and 5, also uses the FPGA and AWG. In this case, the time-scale required to capture the spin order – here given by the inverse of the cantilever frequency $1/f_c$ – must be much shorter than the rotating-frame correlation time τ_m.

[1] Merkulov, I. A., Efros, A. L. & Rosen, M. Electron spin relaxation by nuclei in semiconductor quantum dots. *Phys. Rev. B* **65**, 205309 (2002).

[2] Degen, C. L., Poggio, M., Mamin, H. J., Rettner, C. T. & Rugar, D. Nanoscale magnetic resonance imaging. *Proc. Natl. Acad. Sci. USA* **106**, 1313-1317 (2009).

[3] Xue, F., Weber, D. P., Peddibhotla, P., & Poggio, M. Measurement of statistical nuclear spin polarization in a nanoscale GaAs sample. *Phys. Rev. B* **84**, 205328 (2011).

[4] Mamin, H. J., Rettner, C. T., Sherwood, M. H., Gao, L. & Rugar, D. High field-gradient dysprosium tips for magnetic resonance force microscopy. *Appl. Phys. Lett.* **100**, 013102 (2012).

[5] Mamin, H. J., Oosterkamp, T. H., Poggio, M., Degen, C. L., Rettner, C. T. & Rugar, D. Isotope-selective detection and imaging of organic nanolayers. *Nano Lett.* **9**, 3020-3024 (2009).

[6] Degen, C. L., Poggio, M., Mamin, H. J. & Rugar, D. Nuclear spin relaxation induced by a mechanical resonator. *Phys. Rev. Lett.* **100**, 137601 (2008).

[7] Sidles, J. A., Garbini, J. L. & Drobny, G. P., The theory of oscillator-coupled magnetic resonance with potential applications to molecular imaging. *Rev. Sci. Instrum.* **63**, 3881 (1992).

[8] Mozyrsky, D., Martin, I., Pelekov, D. & Hammel, P. C., Theory of spin relaxation in magnetic

resonance force microscopy. *Appl. Phys. Lett.* **82**, 1278 (2003).

[9] Berman, G. P., Gorshkov, V. N., Rugar, D. & Tsifrinovich, Spin relaxation caused by thermal excitations of high-frequency modes of cantilever vibrations. *Phys. Rev. B* textbf68, 094402 (2003).

[10] Gamliel, D. & Levanon, H., *Stochastic Processes in Magnetic Resonance* (World Scientific, 1995).

[11] Sakurai, J. J., *Modern Quantum Mechanics* (Addison-Wesley, 1994).

[12] Degen, C. L., Poggio, M., Mamin, H. J. & Rugar, D., Role of Spin Noise in the Detection of Nanoscale Ensembles of Nuclear Spins. *Phys. Rev. Lett.* **99**, 250601 (2007).

[13] Rice, S. O. Mathematical analysis of random noise. *AT&T Tech. J.* **23**, 282-332 (1944); *AT&T Tech. J.* **24**, 46-156 (1944).

[14] Assali, S., Zardo, I., Plissard, S., Kriegner, D., Verheijen, M. A., Bauer, G., Meijerink, A., Belabbes, A., Bechstedt, F., Haverkort, J. E. M. & Bakkers, E. P. A. M., Direct Band Gap Wurtzite Gallium Phosphide Nanowires. *Nano Lett.* **13**, 1559 (2013).